HSP90 is a chaperone for DLK and is required for axon injury signaling

Scott Karney-Grobe[a], Alexandra Russo[a], Erin Frey[a], Jeffrey Milbrandt[b,c], and Aaron DiAntonio[a,c,1]

[a]Department of Developmental Biology, Washington University School of Medicine, St. Louis, MO 63110; [b]Department of Genetics, Washington University School of Medicine, St. Louis, MO 63110; and [c]Hope Center for Neurological Disorders, Washington University School of Medicine, St. Louis, MO 63110

Edited by Michael E. Greenberg, Harvard Medical School, Boston, MA, and approved September 4, 2018 (received for review March 27, 2018)

Peripheral nerve injury induces a robust proregenerative program that drives axon regeneration. While many regeneration-associated genes are known, the mechanisms by which injury activates them are less well-understood. To identify such mechanisms, we performed a loss-of-function pharmacological screen in cultured adult mouse sensory neurons for proteins required to activate this program. Well-characterized inhibitors were present as injury signaling was induced but were removed before axon outgrowth to identify molecules that block induction of the program. Of 480 compounds, 35 prevented injury-induced neurite regrowth. The top hits were inhibitors to heat shock protein 90 (HSP90), a chaperone with no known role in axon injury. HSP90 inhibition blocks injury-induced activation of the proregenerative transcription factor cJun and several regeneration-associated genes. These phenotypes mimic loss of the proregenerative kinase, dual leucine zipper kinase (DLK), a critical neuronal stress sensor that drives axon degeneration, axon regeneration, and cell death. HSP90 is an atypical chaperone that promotes the stability of signaling molecules. HSP90 and DLK show two hallmarks of HSP90–client relationships: (*i*) HSP90 binds DLK, and (*ii*) HSP90 inhibition leads to rapid degradation of existing DLK protein. Moreover, HSP90 is required for DLK stability in vivo, where HSP90 inhibitor reduces DLK protein in the sciatic nerve. This phenomenon is evolutionarily conserved in *Drosophila*. Genetic knockdown of *Drosophila* HSP90, Hsp83, decreases levels of *Drosophila* DLK, Wallenda, and blocks Wallenda-dependent synaptic terminal overgrowth and injury signaling. Our findings support the hypothesis that HSP90 chaperones DLK and is required for DLK functions, including proregenerative axon injury signaling.

DLK | HSP90 | injury signaling | axon regeneration | *highwire* ligase

Axon injury occurs in response to trauma, metabolic and toxic insults, and neurodegenerative and genetic diseases. Understanding axonal injury response pathways may lead to strategies for axonal repair. While mammalian central axon regeneration is stunted by a nonpermissive environment and low intrinsic growth capacity (1, 2), peripheral axons can undergo robust regeneration and thus, provide an attractive system to study proregenerative signaling. Peripheral nerve injury activates cytoskeletal remodeling that transforms the injured axon tip into a growth cone (1). Concurrently, local signaling molecules detect the injury and drive retrograde signals to the nucleus to induce expression of regeneration-associated genes (RAGs) (3). This transcriptional program transforms the neuron into a proregenerative state to enable efficient axon regeneration (4, 5).

Dual leucine zipper kinase (DLK) is an essential axon injury sensor and MAP triple kinase that activates the JNK and p38 families (6–8). DLK promotes retrograde transport of injury signals and is required for axon regeneration in mice, *Drosophila*, and *Caenorhabditis elegans* (9–12). Along with DLK, a handful of other kinases, transcription factors, and histone modifiers drive regenerative axon signaling, and other factors are likely yet undiscovered (13–15). We sought to identify additional components of the axon injury response, including previously unidentified pathways or undescribed regulators of known signals, such as DLK. To accomplish this, we developed an in vitro screen to identify injury signals required for induction of the proregenerative program. We took advantage of the preconditioning phenomenon, in which a conditioning injury activates the regeneration program and a second test injury assays its state (16). Traditionally, this paradigm is performed in vivo, but we and others have recently described an in vitro version of this assay in which dissection of mouse dorsal root ganglia (DRG) neurons serves as the preconditioning lesion (17–19). Twenty-four hours later, the regeneration program is active, and we administer the testing injury via replating of the neurons. Preconditioned neurons grow extensive neurites in a short time compared with uninjured neurons. The major advantage that this assay has over the in vivo counterpart is that injury signaling is induced in culture and therefore is amenable to pharmacological perturbations. Importantly, drugs are present only during induction of the regeneration program, not during axon sprouting or outgrowth.

We miniaturized this assay to develop a loss-of-function screening platform to identify small molecules that inhibit induction of the axon regeneration program. From a 480-compound library, we found inhibitors of proteins with no known role in axon injury signaling and inhibitors to several known injury signals. Our analysis focused on the most potent hits, heat shock protein 90 (HSP90) inhibitors, which blocked many of the molecular components of the proregenerative program and the subsequent promotion of robust neurite outgrowth. These phenotypes mimic those seen with loss of DLK. Because HSP90 is a chaperone that facilitates the activity of signaling molecules, including kinases, we tested the hypothesis that HSP90 is required for axon injury signaling as a chaperone for DLK (20, 21). In support of this hypothesis, we show that HSP90 binds DLK and is required for the

Significance

Defining mechanisms of axon injury signaling is critical to understand axon regeneration. This knowledge can be used to develop strategies of axonal repair. Identification of such injury signals has been limited by traditional in vivo assays of proregenerative injury signaling. Here, we describe an in vitro screening platform that specifically identifies proregenerative axon injury signals in mouse neurons. We show that HSP90 is required for injury signaling and detail a mechanism by which HSP90 chaperones the essential proregenerative kinase, dual leucine zipper kinase (DLK). Thus, this work also describes HSP90 as a previously unidentified regulator of DLK, a critical neuronal stress sensor that drives axon regeneration, degeneration, and neurological disease.

Author contributions: S.K.-G., A.R., J.M., and A.D. designed research; S.K.-G., A.R., and E.F. performed research; J.M. contributed new reagents/analytic tools; S.K.-G. and A.R. analyzed data; and S.K.-G. and A.D. wrote the paper.

The authors declare no conflict of interest.

This article is a PNAS Direct Submission.

[1]To whom correspondence should be addressed. Email: diantonio@wustl.edu.

This article contains supporting information online at www.pnas.org/lookup/suppl/doi:10.1073/pnas.1805351115/-/DCSupplemental.

Published online October 1, 2018.

stability of existing DLK protein. We show that HSP90 regulates DLK levels in vivo in mice and *Drosophila*. Moreover, we show that HSP90 is required for both DLK-dependent axon injury signaling and developmental synaptic terminal overgrowth in *Drosophila*. Together, these data demonstrate that DLK is an evolutionarily conserved client of HSP90, that axon injury signaling requires HSP90 activity, and that a primary mechanism by which HSP90 facilitates injury signaling is to chaperone DLK.

Results

A High-Content Loss-of-Function Screen Identifies Potent Disruptors of the Axon Regeneration Program. Peripheral nerve injury stimulates axon regeneration by inducing a proregenerative program. To identify mechanisms by which injury stimulates this program, we used a preconditioning paradigm, in which a first conditioning injury activates the regeneration program and a second test injury assays its state. While preconditioning is traditionally studied in vivo (8, 22), recently, a number of groups have developed in vitro preconditioning assays that take advantage of neuronal replating (17–19). In this method, dissection of the sensory neurons from the animal is the first preconditioning injury, and replating of the neurons 24 h later is the test injury. Axons are then allowed to grow for 18 h, with their length providing a readout for the efficacy of the regenerative program. The major advantage that this assay has over its in vivo counterpart is that injury signaling is induced in culture rather than in an animal and therefore is amenable to pharmacological perturbation. Chemical inhibitors can be applied during the 24-h signaling phase and then washed out before replating, the subsequent test injury (Fig. 1*A*). This enables selective study of proregenerative signaling, not axon sprouting or elongation. We developed a loss-of-function screening platform to identify small molecules that inhibit activators of the axon regeneration program by miniaturizing a previously described replating assay (17). Primary adult DRG neurons were plated, treated with test compounds, replated, stained, and imaged in 96-well plates (Fig. 1*B*). We used a custom high-throughput image analysis pipeline built in CellProfiler to quantify mean total neurite length per neuron for each well (23) (Fig. 1*C*).

We previously showed that pretreatment with JNK inhibitor (JNKi) impairs activation of the regenerative program, leading to reduced axon growth after replating (17). Here, we recapitulate this result in the 96-well format. We included JNKi-treated (positive) and DMSO-treated (negative) control neurons on each screening plate (Fig. 1*B*). DMSO-treated neurons

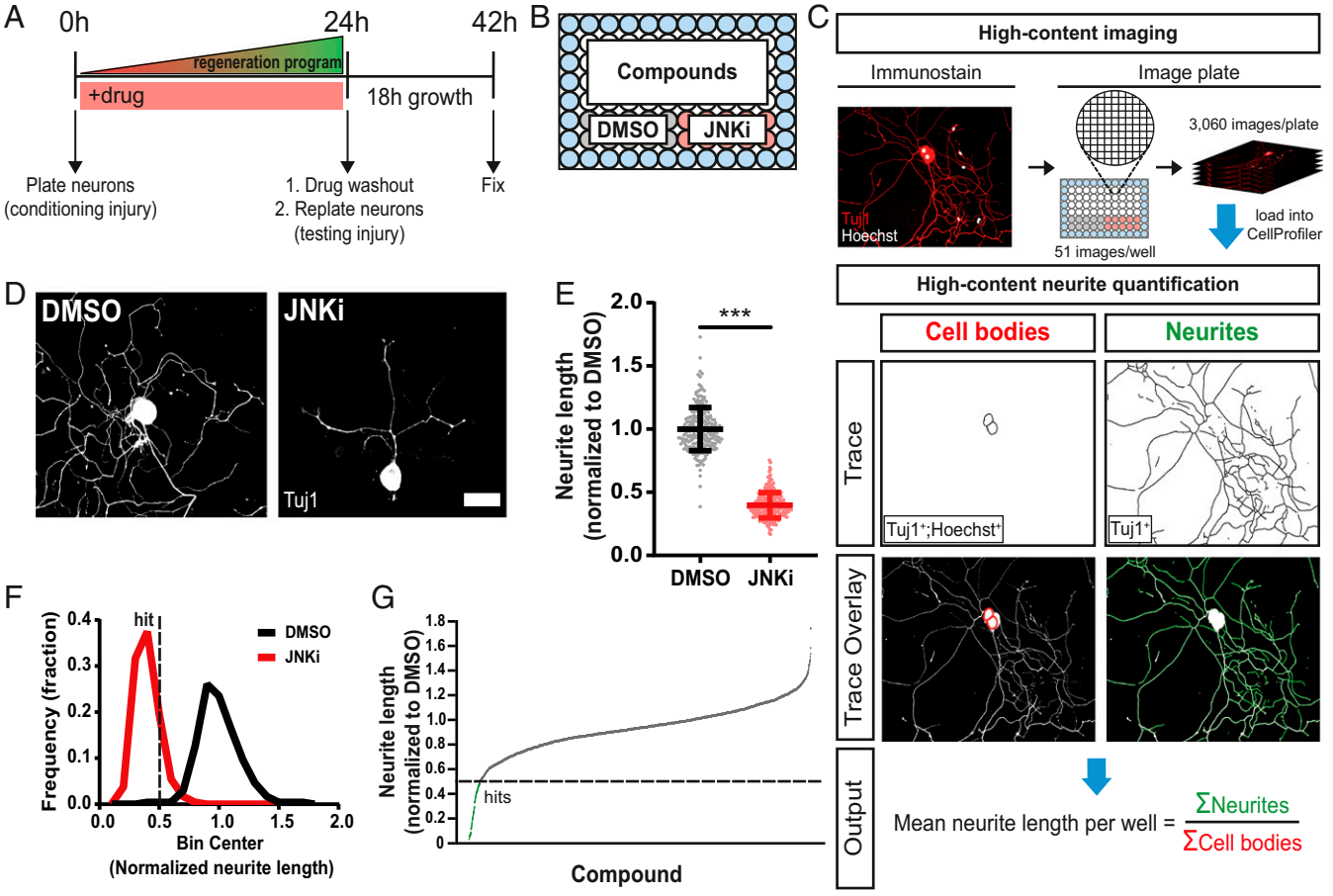

Fig. 1. A loss-of-function screen identifies inhibitors of axon regeneration signaling in vitro. (*A*) Primary adult DRG neurons were harvested and dissociated to activate axon injury signaling (conditioning injury). Immediately after plating into 96-well plates, neurons were treated with compounds. After 24 h, the state of the regeneration program was assessed via a replating (testing injury), and neurons were given 18 h to regrow neurites in the absence of drug. (*B*) Each plate consisted of 60 unique compound wells, 10 wells of the positive control JNKi, and 10 wells of the negative control DMSO. Water (blue) filled the edges of the plate to reduce well-to-well variability. (*C*) Fixed plates were stained for Hoechst and neuronal Tuj1 and imaged on a high-throughput microscope. For each well, total neurite length per cell was quantified using a custom neurite tracing pipeline built in CellProfiler. Within each well, neurite lengths were summed and divided by the total cell count of the well. (*D*) Representative images of screen controls. (Scale bar: 50 μm.) (*E*) Combined data from all control wells in the entire screen: mean ± SD, $n = 238$–240 for each group, unpaired two-tailed t test, $t = 47.1$, df = 476, ***$P < 0.0001$. (*F*) Histogram of *E* with hit cutoff at 0.5 (dotted line). (*G*) Results from screening the ICCB Known Bioactives Library at two doses. Hits are below 0.5 (dotted line).

successfully activated their regeneration program and grew long neurites in the 18-h test phase (Fig. 1 *D* and *E*). JNKi reduced growth by ∼60% compared with DMSO, showing successful inhibition of the regeneration program. DMSO-treated neurons and JNKi-treated neurons formed distinct distributions, showing good separation between control groups (Fig. 1*F*).

To identify other compounds that inhibit induction of the regenerative program, we screened the Institute of Chemistry and Cell Biology (ICCB) Known Bioactives Library (480 compounds) at two doses (*Materials and Methods*). Hits were defined as follows: (*i*) the compound was nontoxic, and (*ii*) the compound caused at least a twofold reduction in growth compared with the negative control [Fig. 1*G*, dotted line (growth cutoff =0.5)]. This minimized the chance of obtaining false positives while maximizing strong true positives (Fig. 1*F*, dotted line). We used final cell count to filter out toxic compounds. Dead or dying cells are washed away during replating, and therefore, wells with toxic compounds have significantly fewer cells than controls. Thus, we defined a compound as toxic if it caused a 50% or more reduction in final neuron count compared with controls (average control cell count =100 neurons per well). Fifty-one unique compounds from the primary screen met the criteria for nontoxic inhibitors of the regeneration program; 45 of these compounds were retested in the 96-well assay, and 35 compounds were hits a second time (*SI Appendix*, Table S1). Of these, we obtained independent lots of seven compounds and successfully validated six using our original assay, in which the longest neurite per neuron is traced by hand (17, 24) (*Materials and Methods*).

The screen produced both known and novel hits (Fig. 1*G* and *SI Appendix*, Table S1). Among the identified compounds known to target proteins with previously characterized roles in injury signaling were our positive control JNKi (SP-600125), rapamycin (mTOR inhibitor), and AG-490 (JAK2 inhibitor) (25, 26). We also found several compounds previously implicated in axon outgrowth or growth cone formation: SB203580 (ERK inhibitor), SB202190 (p38 inhibitor), and roscovitine (CDK inhibitor) (27–29). A prior study showed that DRB (RNA polymerase inhibitor) and LY294002 (PI3K inhibitor) both block induction of the regeneration program in vitro when used at doses similar to those in our screen (18). Although neither compound fell below our hit threshold, both were extremely close, each reducing axonal growth by ∼47%. Despite finding many compounds expected from prior studies, we did not see effects with two PKA inhibitors, H-89 and KT-5720, although PKA is required for injury signaling (30, 31). In addition to these known hits, the screen also identified inhibitors of proteins with no previously described role in proregenerative axon signaling: HSP90, topoisomerase 1 (TOP1), casein kinases (CKs), sarco/endoplasmic reticulum Ca^{2+}-ATPase, and proteases.

HSP90 Inhibition Prevents Activation of the Regeneration Program. From this group of targets, we chose to perform a more detailed characterization of the chaperone HSP90. Two HSP90 inhibitors, geldanamycin and its less toxic analog 17-*N*-allylamino-17-demethoxygeldanamycin (17AAG), were hits at both doses, with the high dose of 17AAG being the number one hit in the screen. Moreover, there is no known role for HSP90 in axon injury signaling or axon regeneration. In the manual replating assay in which the longest neurite per neuron is imaged and quantified by hand, 1 μM 17AAG was sufficient to inhibit the regeneration program over fivefold compared with DMSO-treated controls (Fig. 2 *A* and *B*). To assess whether the block of axon regeneration was due to HSP90 inhibition, we tested a structurally distinct HSP90i, ganetespib (GT), and found that it also blocked preconditioned axon growth. As a comparison, we inhibited the essential proregenerative kinase, DLK, with a recently characterized potent and selective DLK inhibitor (DLKi), GNE-3511 (32), and we found that it also strongly blocked preconditioned axon regrowth. Although 17AAG did not score as toxic in the 96-well format, before proceeding to mechanistic studies, we performed a more rigorous analysis of toxicity by quantifying cell death. Live cells were defined as both positive for the mitochondrial potential marker, Tetramethylrhodamine, methyl ester (TMRM), and negative for the cell death marker, YoPro. Neurons treated with either DMSO or 17AAG for 24 h displayed

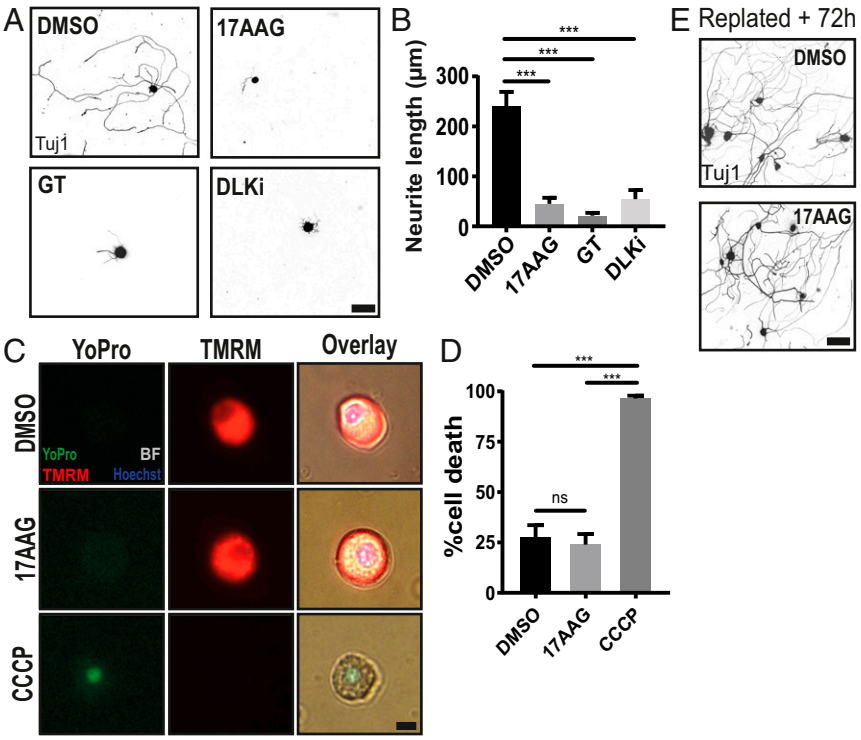

Fig. 2. HSP90 inhibitors potently block induction of the axon regeneration program. (*A*) Low-throughput manual replating assay with the top screen hit 17AAG (1 μM), a structurally different HSP90 inhibitor (15 nM GT), and 500 nM DLK inhibitor GNE-3511 (DLKi). (Scale bar, 100 μm.) (*B*) Quantification of *A* (mean ± SEM). Data represent the mean length of the longest neurite per cell. Within each experiment, two technical replicates (∼100 cells each) were averaged to yield one biological replicate: n = 3–8 independent experiments, one-way ANOVA with Tukey's multiple comparisons, DF = 23, F = 16.2. ***DMSO vs. 17AAG $P < 0.0001$; ***DMSO vs. GT $P < 0.0001$; ***DMSO vs. DLKi $P = 0.0008$. (*C*) Adult DRG neurons cultured for 24 h in the presence of DMSO, 1 μM 17AAG, or 50 μM CCCP (positive control). Cells were loaded with the cell death marker, YoPro, and the mitochondrial potential dye, TMRM, before live imaging. (Scale bar: 10 μm.) (*D*) Quantification of *C* (mean ± SEM). A dead cell was defined as YoPro positive and TMRM negative: n = 3 independent experiments each with 100 cells, one-way ANOVA with Tukey's multiple comparisons, DF = 8, F = 75.3. ns, DMSO vs. 17AAG $P = 0.86$. ***DMSO vs. CCCP $P = 0.0001$; ***17AAG vs. CCCP $P < 0.0001$. (*E*) Neurons pretreated with DMSO or 1 μM 17AAG for 24 h and replated normally but given 72 h to grow neurites rather than 18 h. (Scale bar: 100 μm.) ns, not significant.

~25% cell death, an expected percentage, as not all cells survive dissociation and plating (Fig. 2 *C* and *D*). Those treated with the mitochondrial poison carbonyl cyanide 3-chlorophenylhydrazone (CCCP) were nearly all dead. Lastly, we asked if 17AAG-treated neurons retained the ability to grow neurites long after drug washout to test whether 17AAG permanently abolished the ability of neurons to grow neurites. We performed the replating assay as previously described, but instead of fixing the neurons at 18 h, we fixed at 72 h, allowing ample time for neurons to reactivate their regeneration program and grow long neurites. Indeed, both DMSO-treated and 17AAG-treated neurons grow extensive neurites 72 h after drug washout and replating (Fig. 2*E*). Collectively, these data demonstrate that 17AAG blocks functional activation of the regeneration program and is not toxic to adult sensory neurons.

The axon regeneration program promotes axonal outgrowth via induction of a molecular program that includes transcription factor activation, transcriptional induction of RAGs, and the production of axon growth-associated proteins (4). To explore how HSP90i inhibits the regeneration program, we assessed molecular components of the regeneration program. Twenty-four hours after the conditioning injury, instead of replating the neurons and measuring neurite outgrowth, we quantified the levels of phosphorylated (activated) cJun (p-cJun), up-regulation of regeneration-associated proteins superior cervical ganglion 10 (SCG10) and growth-associated protein 43 (GAP43), and transcriptional induction of two RAGs: *Small proline-rich protein 1a* (*Sprr1a*) and *Galanin*. cJun is the transcription factor target of JNK, and it promotes axon regeneration (33). cJun phosphorylation increased approximately fivefold between 1 and 24 h postplating (Fig. 3 *A* and *B*). Neurons treated with 17AAG only increased their p-cJun signal 1.6-fold. As a positive control, we tested the effect of DLKi, since DLK is required for cJun phosphorylation after peripheral nerve injury in vivo (8). As expected, application of DLKi blocks the phosphorylation of cJun in this system. SCG10 and GAP43 are injury-induced cytoskeletal remodelers that are commonly used molecular markers of regenerating axons (10, 17). In neurons cultured for 24 h, SCG10 and GAP43 increased approximately 7- (Fig. 3 *A* and *C*) and 2.5-fold (Fig. 3 *A* and *D*), respectively. Surprisingly, neither 17AAG nor DLKi had a significant effect on the induction of these proteins. *Sprr1a* and *Galanin* are injury-induced transcripts that each encode axon growth proteins (33, 34). At 24 h after plating, both *Sprr1a* and *Galanin* are robustly up-regulated (Fig. 3*E*). Neurons treated with 17AAG or DLKi fail to up-regulate these genes in response to axon injury. Hence, inhibition of HSP90 potently suppresses axonal outgrowth after injury while

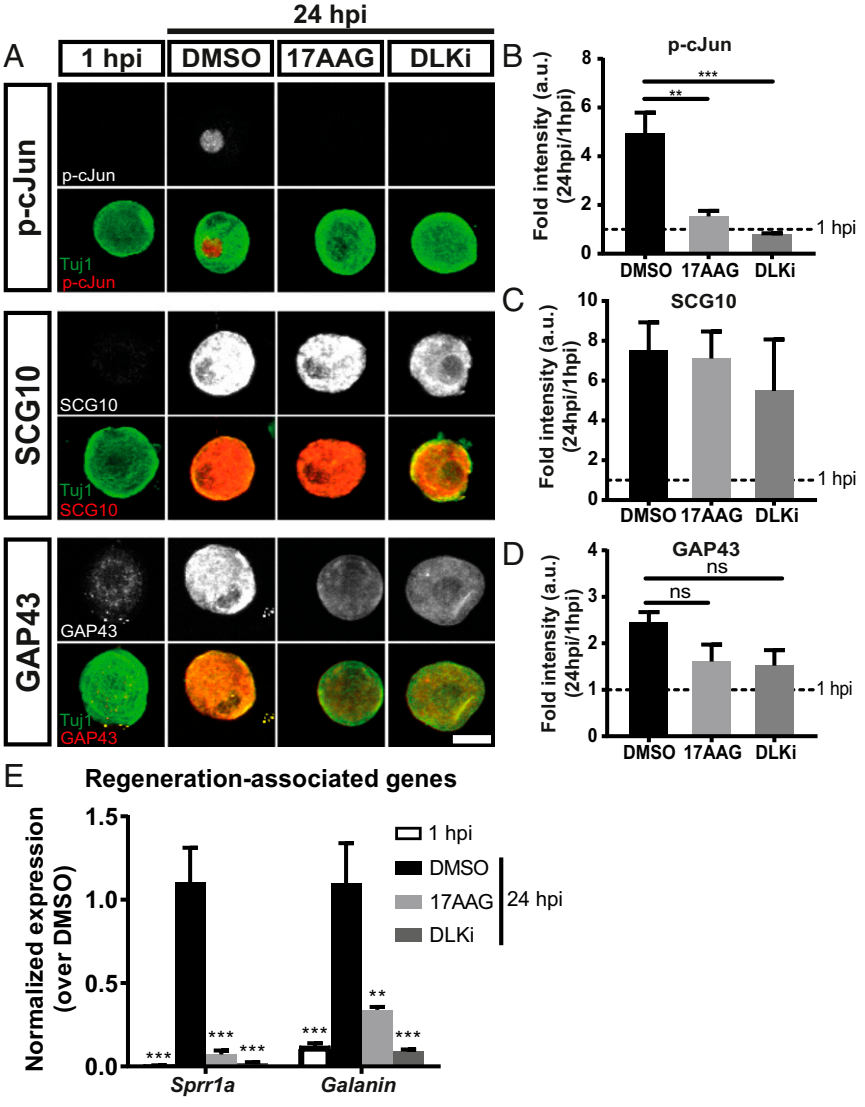

Fig. 3. Inhibition of HSP90 blocks molecular components of the axon regeneration program. (*A*) Adult DRG neurons plated and treated with DMSO, 1 μM 17AAG, and 500 nM DLKi. At 24 h postinjury (hpi), adult DRG neurons were fixed and immunostained for proregenerative markers (gray in *Top* and red in merged) and neuronal Tuj1 (green). (Scale bar: 20 μm.) (*B–D*) Quantification for each marker (mean ± SEM). Fold intensity was normalized to neurons at 1 hpi ("uninjured"): $n = 3$–5 independent experiments with ~40 neurons quantified per group per experiment, one-way ANOVA with Tukey's multiple comparison test. (*B*) DF = 17, $F = 15.3$, DMSO vs. 1 hpi $P = 0.0002$. $^{**}P = 0.001$ DMSO vs. 17AAG; $^{***}P = 0.0006$ DMSO vs. DLKi. (*C*) DF = 14, $F = 6.64$, DMSO vs. 1 hpi $P = 0.01$, DMSO vs. 17AAG $P = 0.99$, DMSO vs. DLKi $P = 0.80$. (*D*) DF = 14, $F = 7.15$, DMSO vs. 1 hpi $P = 0.004$, DMSO vs. 17AAG $P = 0.099$, DMSO vs. DLKi $P = 0.09$. (*E*) Adult DRG neurons were dissociated, plated, and treated with 1 μM 17AAG, 500 nM DLKi, or DMSO. At 24 hpi, RNA was collected, and RAGs were analyzed via qRT-PCR. Fold intensity was normalized to DMSO-treated neurons at 24 hpi: mean ± SEM, $n = 5$–8 independent experiments, one-way ANOVA with Tukey's multiple comparison test. For *Sprr1a*, DF = 26, $F = 19.8$. $^{***}P < 0.0001$ DMSO vs. 1 hpi; $^{***}P < 0.0001$ DMSO vs. 17AAG; $^{***}P < 0.0001$ DMSO vs. DLKi. For *Galanin*, DF = 18, $F = 14.0$. $^{**}P = 0.003$ DMSO vs. 17AAG; $^{***}P = 0.0005$ DMSO vs. 1 hpi; $^{***}P = 0.0002$ DMSO vs. DLKi. ns, not significant.

blocking some but not all molecular components of the regeneration program. HSP90 inhibitor is not poisoning the entire regenerative program; instead, it may inhibit specific signaling pathways.

HSP90 Binds DLK. HSP90 is a chaperone that regulates the stability, localization, or activity of signaling molecules (21). Given the large number of HSP90 clients, HSP90 may chaperone multiple axon injury signals. The similarity of HSP90i and DLKi phenotypes led us to hypothesize that DLK may be one such HSP90 client. Moreover, DLK is an essential proregenerative molecule, and therefore, this could be one mechanism by which HSP90 facilitates axon injury signaling. An HSP90–client relationship is characterized by two key features: (*i*) the two proteins physically interact, and (*ii*) the client protein is degraded with loss of chaperone function (35). To investigate whether HSP90 binds DLK, we expressed flag-tagged DLK in HEK-293 cells, which do not normally express DLK, prepared lysate, and immunoprecipitated DLK using anti-flag antibody. Endogenous HSP90 was strongly enriched in the pull-down from cells expressing DLK but not in lysate from cells lacking DLK (Fig. 4*A*). Next, we sought to test for this interaction in DRG neurons. We collected lysate from wild-type, uninjured DRG neurons and immunoprecipitated endogenous DLK with an anti-DLK antibody. Endogenous HSP90 is coimmunoprecipitated with DLK, indicating that HSP90 and DLK interact in neurons under baseline conditions (Fig. 4*B*). This finding is supported by a prior large-scale HSP90 interactome screen, in which immobilized DLK captured HSP90 protein (36). These data reveal an HSP90–DLK interaction, supporting the hypothesis of a chaperone–client relationship.

HSP90 Is Required for DLK Stability. A second major hallmark of an HSP90–client relationship is loss of client stability during chaperone inhibition. Thus, if HSP90 is a chaperone for DLK, HSP90i should lead to DLK degradation. To test this, we measured DLK protein levels in DRG neurons with and without HSP90 inhibition. Inhibition of HSP90 caused a 3.5-fold decrease in DLK protein after 8 h compared with treatment with DMSO vehicle (Fig. 5 *A* and *B*). To test whether HSP90 chaperones other MAPKs in the DLK pathway, we probed for the MAPKs downstream of DLK: MKK4 and JNK (37). Consistent with published data, MKK4 and JNK protein levels were unaffected by HSP90i (36, 38). There are two explanations for this DLK phenotype. (*i*) Existing DLK requires HSP90 for stability but is degraded when HSP90 is inhibited. Or, (*ii*) HSP90 functions as a traditional protein folding chaperone to facilitate synthesis of new DLK, and therefore, HSP90 inhibition would block production of new DLK. For this latter possibility to explain the rapid drop in DLK levels with HSP90 inhibition, preexisting DLK must be rapidly turned over. If so, then DLK levels should decline to a similar extent when production is blocked via an independent method, such as inhibition of protein synthesis. To test this second model, we blocked protein synthesis with cycloheximide and assessed DLK protein levels. We detect no significant change in DLK protein levels after 8 h of treatment (Fig. 5 *C* and *D*). To confirm that cycloheximide was effectively blocking protein synthesis, we quantified the levels of the labile protein SCG10 (37, 39) and saw a rapid, near-complete depletion of SCG10 after cycloheximide treatment. Thus, within an observation period of 8 h, DLK protein is stable in cultured DRG neurons. On application of HSP90 inhibitor, however, this existing pool of DLK protein is rapidly lost.

Next, we tested whether HSP90 is required for DLK stability in vivo. To acutely inhibit HSP90 in mammals, we injected adult mice i.p. with 75 mg/kg 17AAG or DMSO vehicle three times a day for 2 d. Three hours after the final injection, we collected sciatic nerve for protein analysis. The sciatic nerve of mice treated with 17AAG had ∼50% less DLK protein than nerves from DMSO-treated mice (Fig. 5 *E* and *F*). This effect is not quite as dramatic as in cultured neurons, possibly because 17AAG has a half-life of under 1 h in plasma (40). As seen in vitro, MKK4 and JNK protein levels were unchanged with HSP90i in vivo. Together, these data demonstrate that HSP90 binds to DLK and that HSP90 is required for DLK stability both in cultured neurons and in vivo, supporting the hypothesis that DLK is a client of HSP90. Furthermore, within the DLK MAPK pathway, HSP90 specifically chaperones DLK.

The *Drosophila Hsp90* Ortholog, *Hsp83*, Is Required for DLK Stability and Axon Injury Signaling in Vivo. Having shown that HSP90 function is required for axon injury signaling and DLK stability in mammals, we turned to a *Drosophila* axon injury model for genetic validation and to test whether this mechanism is evolutionarily conserved. As in mammals, *Drosophila* axon injury triggers a DLK–JNK retrograde signal that activates a transcriptional regeneration program (6, 12, 41). We first asked whether levels of the fly ortholog of DLK, Wallenda (Wnd), were affected by loss of Hsp83, the *Drosophila* ortholog of HSP90. We expressed either RFP (control) or an RNAi transgene targeting *hsp83* in the nervous system of larvae before harvesting the ventral nerve cord (VNC) for protein analysis. This RNAi transgene is effective, leading to an approximately fivefold reduction in Hsp83 protein levels (Fig. 6 *A* and *B*). In larvae expressing the *hsp83* RNAi transgene, there is a concomitant approximately twofold reduction in the levels of Wnd protein compared with in control animals (Fig. 6 *A* and *C*). Thus, loss of Hsp83 protein, like inhibition of HSP90 in mammals, causes a loss of total Wnd protein in *Drosophila*.

To investigate the role of *hsp83* in *Drosophila* axon injury signaling, we quantified injury-induced JNK activation, a DLK-dependent phenomenon. JNK activity can be quantified in *Drosophila* with a nuclear LacZ enhancer trap inserted into the JNK phosphatase *puckered* (*puc*-LacZ), a JNK transcriptional target (42). Normally, JNK activity is minimal, leading to low expression of *puc*-LacZ. Injury-induced JNK activation drives a dramatic increase in *puc*-LacZ (12). We assessed the levels of *puc*-LacZ in larvae expressing neuron-specific RNAi transgenes targeting *white* (control), *hsp83*, or *wnd*. Twenty-four hours after crushing motor neuron axons, there is an eightfold increase in *puc*-LacZ in control neurons (Fig. 6 *D* and *E*). Knockdown of *hsp83* or *wnd* strongly inhibits this response. Together, these data show that Hsp83 is required for DLK stability and injury signaling in vivo and suggest the DLK–HSP90 client–chaperone relationship is evolutionarily conserved from mammals to invertebrates.

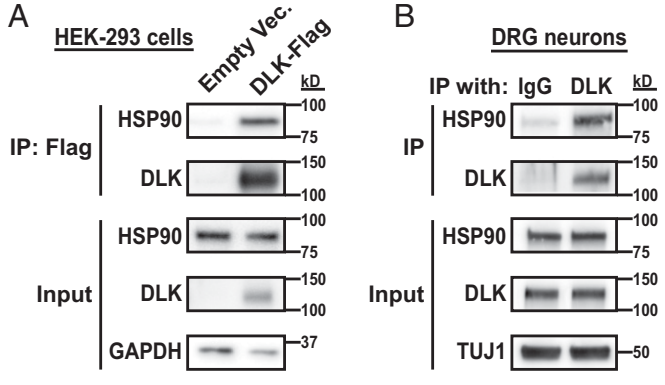

Fig. 4. HSP90 binds DLK. (*A*) Empty vector or Flag-tagged DLK plasmids were expressed in HEK-293 cells before DLK was immunoprecipitated with anti-flag beads. The precipitates were probed for endogenous HSP90. Input represents 1% of total lysate collected before immunoprecipitation (IP). Data are from one representative experiment of $n = 5$ individual experiments. (*B*) Wild-type embryonic DRG neurons were cultured for 6 d, lysed, and incubated with either IgG or anti-DLK antibody to immunoprecipitate endogenous DLK. Precipitates were probed for endogenous HSP90. Input represents 1.7% of total lysate collected before IP.

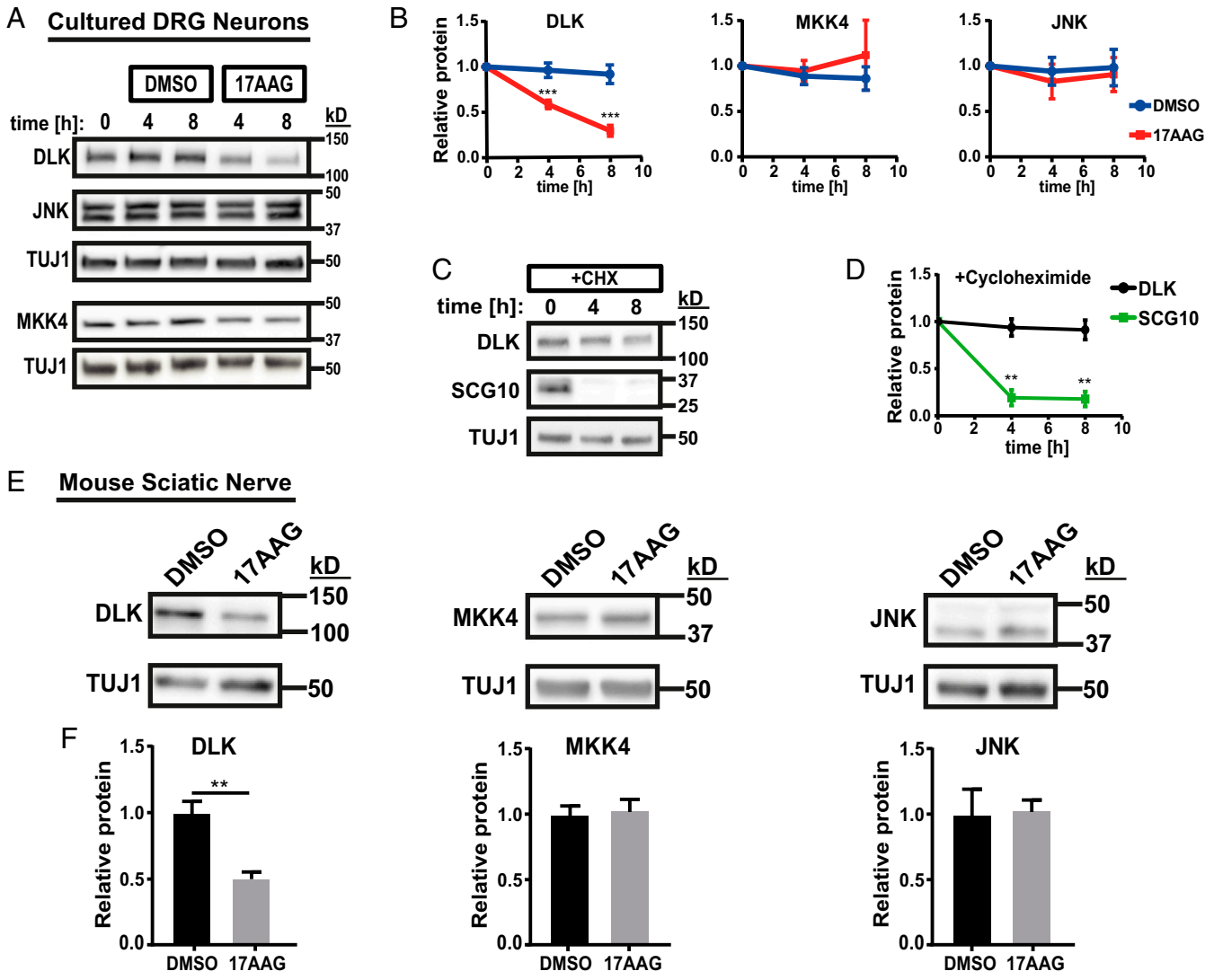

Fig. 5. HSP90 inhibition in mouse neurons causes DLK protein degradation in vitro and in vivo. (*A*) Embryonic DRG neurons were cultured for 6 d and then treated with either DMSO or 5 μM 17AAG. Lysate was collected after 0, 4, or 8 h of treatment and probed for DLK, JNK, MKK4, and TUJ1 (loading control). To avoid excessive stripping, lysates were rerun to probe for JNK or MKK4. The representative MKK4 bands are depicted with their respective TUJ1 loading controls. (*B*) Quantification of *A* (mean ± SEM). Band intensity was normalized to the 0-h time point. Two-way ANOVA with Sidak's multiple comparisons test. (*Left*) DLK: $n = 6$ independent experiments; time: DF = 2, $F = 36.1$; treatment: DF = 1, $F = 23.9$. ***$P = 0.0005$ DMSO vs. 17AAG at 4 h; ***$P < 0.0001$ DMSO vs. 17AAG at 8 h. (*Center*) MKK4: $n = 4$ independent experiments; time: DF = 2, $F = 0.17$; treatment: DF = 1, $F = 0.38$. DMSO vs. 17AAG at 4 h $P = 0.99$; DMSO vs. 17AAG at 8 h $P = 0.68$. (*Right*) JNK: $n = 3$ independent experiments; time: DF = 2, $F = 0.54$; treatment: DF = 1, $F = 0.14$. DMSO vs. 17AAG at 4 h $P = 0.94$; DMSO vs. 17AAG at 8 h $P = 0.98$. (*C*) To determine if DLK is turned over within 8 h, neurons were treated with cycloheximide (CHX) for the indicated times. Lysate was probed for DLK and the labile protein SCG10 (protein turnover control). (*D*) Quantification of *C* (mean ± SEM). Band intensity was normalized to the 0-h time point. $n = 5$ independent experiments; two-way ANOVA with Sidak's multiple comparisons test; time: DF = 2, $F = 28.4$; protein: DF = 1, $F = 51.6$. DLK: 0 vs. 4 h $P = 0.89$; 0 vs. 8 h $P = 0.83$. SCG10: **$P = 0.002$ 0 vs. 4 h; **$P = 0.002$ 0 vs. 8 h. (*E*) Adult mice were injected i.p. with 75 mg/kg 17AAG or DMSO three times per day for 2 d before collection of sciatic nerve lysate. Representative images from one pair of mice. (*F*) Quantification of *E* (mean ± SEM). Band intensity was normalized to DMSO controls. $n = 4$ mice per condition; unpaired two-tailed *t* test. (*Left*) DLK: $t = 4.4$, df = 6. **$P = 0.004$. (*Center*) MKK4: $t = 0.25$, df = 6. $P = 0.81$. (*Right*) JNK: $t = 0.14$, df = 6. $P = 0.89$.

Hsp90 Is Required for Developmental DLK Signaling. Lastly, we tested whether HSP90 only stabilizes DLK in the context of injury or whether HSP90 is required for Wnd/DLK signaling more broadly. DLK is a critical protein not only for axon regeneration but also for neural development and neurodegeneration (2, 15, 43). We first assessed synapse growth in *Drosophila*, a well-established phenotype for Wnd (DLK). Wnd/DLK drives the dramatic synaptic terminal overgrowth in mutants for *highwire* (*hiw*), which encodes the ubiquitin ligase that targets Wnd/DLK (43, 44). At the *Drosophila* larval neuromuscular junction (NMJ), *hiw* mutants display overgrown synaptic terminals with nearly four times as many synaptic boutons as wild-type controls. As previously shown, RNAi to *wnd* completely suppresses this phenotype. We observed an equally potent suppression of the overgrowth phenotype when knocking down *hsp83* (Fig. 7).

Finally, we asked if HSP90 is also required for developmental DLK signaling in mammalian neurons after trophic factor withdrawal. Depriving embryonic DRG neurons of nerve growth factor (NGF) triggers DLK-dependent cJun phosphorylation (45). We pretreated neurons with either DMSO or HSP90i for 8 h to deplete DLK before NGF withdrawal. Three hours post-NGF deprivation, we assessed phosphorylated cJun. Similar to DLK inhibition, HSP90 inhibition potently blocked cJun activation induced by NGF deprivation (*SI Appendix*, Fig. S1). Together with

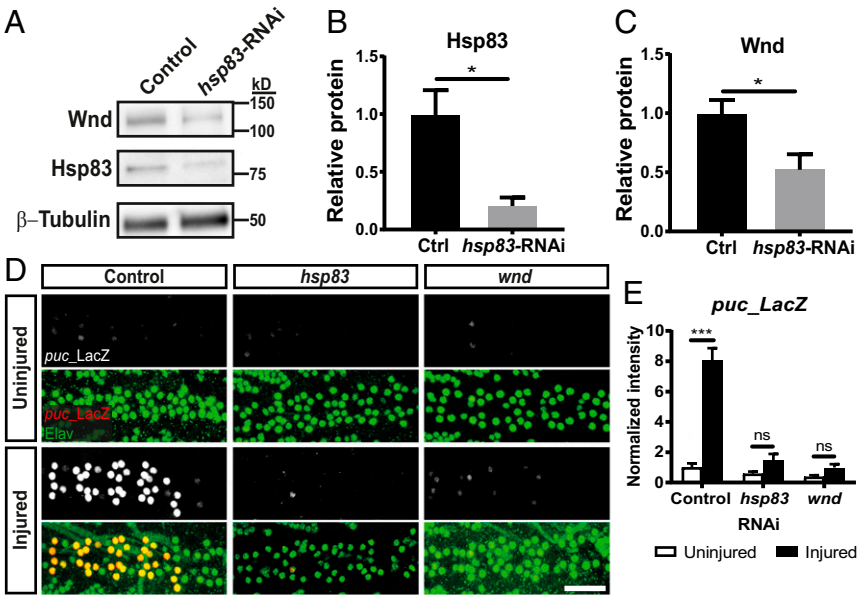

Fig. 6. The *Drosophila Hsp90* ortholog, *hsp83*, is required for DLK stability and injury-induced JNK signaling in vivo. (*A*) Representative Western blot of protein lysate from VNCs of *elav3E-Gal4;UAS-RFP* (control) or *elav3E-Gal4;UAS-hsp83-RNAi* (*hsp83*-RNAi) *Drosophila* third-instar larvae. Lysate was probed for the fly ortholog of DLK, Wnd, and Hsp83. (*B* and *C*) Quantification of *A* (mean ± SEM). Band intensities were normalized to controls. $n = 4$ experiments per genotype, where each experiment consisted of 10 VNCs pooled into one lysate; unpaired two-tailed *t* test. (*B*) $t = 3.36$, df = 6. $^*P = 0.015$. (*C*) $t = 2.57$, df = 6. $^*P = 0.042$. (*D*) Ventral motor neurons of third-instar larvae were crushed with forceps and fixed 24 h later. Representative images of the VNC midline of *BG380-Gal4;puc*-LacZ/*UAS-white-RNAi* (control), *BG380-Gal4;puc*-LacZ/*UAS-hsp83-RNAi* (*hsp83*), and *BG380-Gal4;puc*-LacZ/*UAS-wnd-RNAi* (*wnd*) larvae stained for puc-LacZ expression (red) and elav (green) to identify motor neuron nuclei. (Scale bar: 25 μm.) (*E*) Quantification of *D* (mean ± SEM). $n = 7$–13 animals per group, where a group is defined as one genotype plus injury combination (i.e., six total groups); one-way ANOVA with Tukey's multiple comparisons test; DF = 49, $F = 39.0$. $P = 0.88$ hsp83 uninjured vs. injured; $P = 0.98$ wnd uninjured vs. injured. $^{***}P < 0.0001$ control (ctrl) uninjured vs. injured. ns, not significant.

the data from *Drosophila*, these findings support the hypothesis that the HSP90–DLK chaperone–client relationship impacts DLK signaling broadly and is not restricted to axon injury signaling.

Discussion

We performed a screen in primary adult mouse neurons to identify additional axon injury signals and found that HSP90 is required for injury to induce the proregenerative program in mouse and *Drosophila* neurons. Data from mechanistic experiments support the model that HSP90 promotes axon injury signaling, at least in part, by chaperoning DLK. In neurons, HSP90 binds DLK, maintains DLK protein levels, and is required for DLK activity, such as JNK activation and RAG induction after axon injury and synaptic overgrowth during development.

An in Vitro Preconditioning Assay to Screen for Proregenerative Axon Injury Signals. Numerous screens have identified the transcription factors and RAGs that compose the axon regeneration program and its output of cytoskeletal remodelers, axon growth molecules, and guidance proteins (13, 46–52). These efforts have defined critical components of the axon regeneration process and have led to promising translational results, including growth onto inhibitory substrates and CNS axon regeneration in vivo (46, 52). Here, we contribute to these efforts by probing for injury-activated proteins that induce the proregenerative program in primary mammalian neurons. We performed an in vitro screen that uses preconditioned neurite outgrowth as a functional readout to test 480 compounds for the ability to prevent injury from activating the proregenerative program. Our assay is unique in that it distinguishes components of the induction phase, during which injury signals activate the program. Because this induction occurs in culture, we can apply small molecule inhibitors and wash them out before the testing injury (replating). As a result, neurons regenerate neurites in the absence of perturbation; only the induction phase was manipulated. Thus, this assay allows us to specifically target injury signals that induce the proregenerative program and avoid affecting its products, such as axon elongation or growth cone proteins.

In this screen, we identified 35 compounds that reduced preconditioned neurite regeneration by at least twofold. The robustness of our screen is highlighted by hits that were known injury signals. For example, AG490 (Janus kinase 2 inhibitor) and rapamycin (mTOR inhibitor) were previously shown to inhibit preconditioning when injected into mice (25, 26). Other hits, such as ERK and GSK3 inhibitors, support studies showing that genetic loss of either protein impairs mammalian axon regeneration (18, 53). Lastly, roscovitine, a CDK5 inhibitor and potent hit in our screen, inhibited axon regeneration when applied after injury to the rat facial nerve in vivo (27). This study also described accumulation of CDK5 in regenerating axons. Our data suggest an additional role for CDK5 as an injury signal that induces the proregenerative program. Our p38 inhibitor (SB203580, SB202190) results provide mammalian data in support of previous findings that show that *C. elegans* and *Drosophila* p38 orthologs are required for axon injury signaling (6, 54). In addition to HSP90, our screen also identified many previously unclassified injury signal candidates, including TOP1, CKs, CDKs, and the proteasome, although genetic validation is required before follow-up. Indeed, our capsazepine hit suggested that TRPV1 is necessary to induce the regeneration program; however, we found that capsazepine still inhibited preconditioned neurite regrowth in TRPV1 knockout neurons, showing that this is an off-target effect. Interestingly, using a similar screening approach, our group recently showed that TRPV1 activation is sufficient to induce the regeneration program in small diameter sensory neurons (55). Lastly, several hits, such as curcumin or resveratrol, target dozens of proteins and thus provide little mechanistic information. Indeed, the utility of this assay depends on the specificity of compounds screened.

Recently, a similar high-content screen was performed in zebrafish (56). Larval motor axons were axotomized via fin

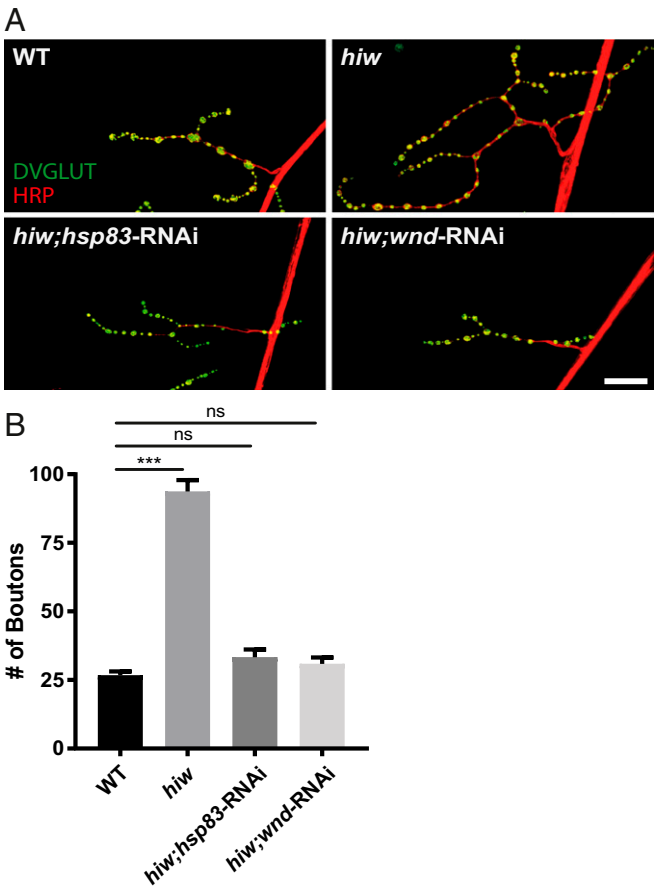

Fig. 7. HSP90 is required for DLK-dependent synaptic terminal overgrowth at the *Drosophila* NMJ. (*A*) Representative images of third-instar larva muscle 4 NMJs of wild-type (WT); *hiw*; *highwire*^{ND9},*dvglut-Gal4;UAS-wallenda-RNAi* (*hiw;wnd*-RNAi); and *highwire*^{ND9},*dvglut-Gal4;UAS-hsp83-RNAi* (*hiw;hsp83*-RNAi) animals stained for the presynaptic bouton marker DVGLUT (green) and nerve membrane marker HRP (red). (Scale bar: 25 μm.) (*B*) Quantification of *A* (mean ± SEM). n = 18–23 NMJs total from at least four animals per genotype; one-way ANOVA with Tukey's multiple comparisons test; DF = 78, $F = 128.6$. $P = 0.69$ WT vs. *hiw;wnd*-RNAi; $P = 0.30$ WT vs. *hiw;hsp83*-RNAi. ***$P < 0.0001$ WT vs. *hiw*. ns, not significant.

amputation before a 24-h incubation with the ICCB Known Bioactives library, the same library that we used. Our assays differed in that our compounds were only present during the induction phase of injury signaling, while in the study by Bremer et al. (56), compounds were present during the induction and outgrowth phases. Despite these differences, both studies share many validated hits, including JNKi (SP600125), both p38 inhibitors (SB202190, SB203580), and the CDK inhibitor roscovitine. The concordant findings of these known signals highlight the robust nature of both assays. One top hit shared by both screens was the TOP1 inhibitor, camptothecin. Interestingly, their data suggest a role for TOP1 in promoting Schwann cell survival after injury. Our in vitro assay is performed in the absence of Schwann cells, leading us to hypothesize that TOP1 is also required in neurons to activate the proregenerative program. Lastly, several hits were not shared between the two screens, including HSP90, which was toxic in the zebrafish screen and therefore was not analyzed. There are several reasons that compounds may only have been hits in one screen, including technical differences, such as the presence of drug during the axon outgrowth phase in the zebrafish screen, the possibility of noncell autonomous effects in vivo, dosing and/or drug metabolism differences, or discordant mechanisms of zebrafish and mouse axon injury signaling. Overall, both screens provide unique advantages to identify components of axon regeneration and injury signaling.

A Role for HSP90 in Axon Injury Signaling. Traditional chaperones, such as the HSP60, HSP70, and HSP100 families, drive protein folding, disaggregation, and proteolysis (57). HSP90, however, facilitates maturation, complex assembly, localization, and ligand binding of signal transduction proteins, including kinases and nuclear receptors (21). Given the role of HSP90 in many signaling hubs, it is not surprising that HSP90 inhibitors were the top hits in our screen. While HSP90 has many targets, the efficacy of HSP90 inhibition in our injury assays can be, in part, explained by its regulation of DLK, an essential injury signal. Due to the number of clients, it is unlikely that DLK is the only injury signal chaperoned by HSP90. Indeed, it was recently shown that HSP90 physically interacts with over one-half of the human kinome (36). Nonetheless, those authors found no interaction between HSP90 and many other injury-associated MAPKs, such as leucine zipper kinase, MKK7, JNK1-3, and ERK1/2. Our data showing that MKK4 and JNK protein levels are unaffected by HSP90i agree with this published data (Fig. 5*B*). In addition, the fact that HSP90i does not significantly influence up-regulation of SCG10 or GAP43 (Fig. 3) suggests that the role of HSP90 is confined to specific injury pathways. In future studies, it will be interesting to identify any remaining HSP90 clients within the context of axon injury.

HSP90 has established roles in other neuronal contexts, namely the stabilization of neurodegenerative protein aggregates, but also, in neuronal polarization, axon pathfinding, and neurotransmitter release (58–61). Here, we describe a role for HSP90 in axon injury signaling and synapse growth. Other HSPs, HSP27 and HSP70, are up-regulated after axon injury and localize to axons, and HSP27 promotes axon outgrowth (62, 63). Interestingly, local translation of HSP90, HSP70, and HSP27 has been observed in injured DRG neurons in vitro (63). Thus, HSPs likely play a vital role at many stages of axon regeneration.

A Mechanism of DLK Regulation: HSP90 Chaperone Activity. Intense efforts to understand mechanisms of DLK regulation are driven by the central role that DLK plays in neuronal stress, development, axon regeneration, axon degeneration, and neurodegenerative disease (2, 7, 8, 11, 15, 45, 64, 65). Neuronal DLK can be activated directly by Ca^{2+} in *C. elegans*, cytoskeletal disruption, cAMP/PKA in *Drosophila* and mammals, and by increasing DLK protein levels (24, 30, 41, 43, 66). To date, the best understood mechanism for regulating DLK is controlling its abundance. The best-known regulator of DLK abundance is the E3 ubiquitin ligase, PHR1/hiw/RPM-1, which actively targets DLK for degradation in mice, *Drosophila*, and *C. elegans* (43, 67–69). After injury, PHR1/hiw levels decrease to promote increased DLK levels (12). In addition, mammalian DLK drives a positive feedback loop in which its downstream MAPK, JNK, phosphorylates DLK to protect it from ubiquitination via PHR1 (70). Here, we identify HSP90 as an additional factor regulating DLK abundance: HSP90 is required to stabilize the existing pool of DLK protein. Loss of HSP90 activity, either via inhibition in mice or genetic knockdown in *Drosophila*, drives a sudden decline in DLK protein abundance. One major question that remains is whether HSP90's interaction with DLK is regulated. Our data suggest that the HSP90–DLK interaction exists before injury, because in uninjured neurons, DLK and HSP90 coimmunoprecipitate and HSP90i depletes existing DLK protein. Nonetheless, this interaction could be modulated by injury, thus protecting DLK from degradation by blocking ubiquitination via PHR/Hiw or promoting the JNK-mediated feedback loop. Hence, our identification of an evolutionarily conserved mechanism by which HSP90 regulates levels of DLK protein adds to our molecular understanding of DLK-dependent neuronal stress signaling and its regulation in development and disease.

Materials and Methods

Mice and Primary DRG Neuron Culture. Adult CD1-IGS mice were purchased from Charles River. All experiments were performed with male and female mice ages 8–12 wk old. Mouse husbandry was performed under the supervision of the Washington University Division of Comparative Medicine. Adult and embryonic DRG neurons were isolated and cultured as previously described (17, 24). All experiments in this study using mice were reviewed and approved by the Washington University School of Medicine Institutional Animal Care and Use Committee. Detailed procedures can be found in *SI Appendix*.

Replating Assay and Neurite Length Analysis. Replating was performed as previously described (17). Medium (including any drug treatment) was removed, and cells were briefly washed with warmed DMEM before a 5-min incubation with 0.025% trypsin-EDTA. Trypsin was replaced with fresh culture media, and the plate was gently washed several times to release neurons before the entire cell suspension was replated onto poly-D-lysine (PDL) and laminin-coated glass chamber slides. After 18 h, neurons were fixed and stained for Tuj1. Tuj1-positive neurons were imaged at 10×, and the longest neurite of each neuron was traced using the ImageJ plugin NeuronJ (71). Within each experiment, two technical replicates (~100 cells each) were averaged to yield one biological replicate. Data represents three to eight independent experiments. Detailed procedures can be found in *SI Appendix*.

Automated Replating Assay, Imaging, and Neurite Length Analysis. Adult DRG neurons were plated into PDL/laminin-coated 96-well plates (Corning). Neurons were plated at a density such that cells from one mouse filled two 96-well plates. The inner 60 wells received cells, while the outermost wells were filled with water to reduce plate-to-plate variability caused by evaporation. Replating, fixing, and staining were performed as previously described but with a 12-span pipette. Plates were imaged on an Operetta High-Content Imaging System (Perkin-Elmer) with a 20× long-working distance air objective. The entirety of each well was imaged, giving 51 images per well. The images were run through an automated image analysis pipeline that we built in CellProfiler (23) (Fig. 1*C*). In brief, the pipeline identifies Hoechst-positive and Tuj1-positive neuronal somas and Tuj1-positive neurites. It skeletonizes the image, subtracts the somas, and measures total length of the remaining neurites. For each well, dividing the sum neurite length by the total neuronal soma count gave mean neurite length per neuron. Within each plate, mean neurite length values were normalized to the average of the 10 negative (DMSO) controls.

Pharmacology. The Screen-well ICCB Known Bioactives Library (Enzo) was purchased from the Washington University High-Throughput Screening Core. The library consisted of 480 compounds dissolved in DMSO. We screened each compound at two concentrations between 100 nM and 100 μM, with most between 1 and 20 μM. Compounds were applied to cells immediately after plating for 24 h and were washed off before replating.

SP600125 (JNKi; Sigma) was used at 15 μM in all experiments; 17AAG (ApexBio) was used at 1 μM on adult DRG neurons and 5 μM on embryonic DRG neurons. GNE-3511 (DLKi; MedChem Express) was used at 500 nM. GT (ApexBio) was used at 15 nM. CCCP (Sigma) was used at 50 μM. DMSO was the vehicle for all drugs in this study except cycloheximide (Sigma), which was dissolved into ethanol and applied at 500 μg/mL final.

To administer 17AAG in vivo, a 50-mg/mL stock of 17AAG was made in DMSO, and mice were injected i.p. at 75 mg/kg. Mice were injected three time per day for 2 d, with injections roughly 4 h apart and administered on alternating sides of the abdomen; 3–4 h after the final injection, sciatic nerves were collected for Western blot analysis.

Immunocytochemistry. Neurons were fixed with 4% paraformaldehyde, blocked, and incubated with primary antibody overnight. After washes, secondary antibodies were applied, and slides were washed again before mounting and imaging. Detailed procedures, including all antibodies used, can be found in *SI Appendix*; 30–50 Tuj1-positive neurons were imaged per group for each experiment, and intensities were quantified in ImageJ. Within one experiment, all images were taken with the same gain, and each group was normalized to the 1-h baseline intensity; $n = 3$–5 independent experiments were performed.

Cell Death Analysis. Adult DRG neurons were plated and treated with DMSO, 17AAG, or CCCP. After 22 h, cells were loaded with 50 nM TMRM, 1 μM Yo-Pro-1, and 500 ng/mL Hoechst 33342 (all dyes from Life Technologies). At 24 h, the cells were placed in a CU-501 live-imaging chamber (Live Cell Instrument) maintained at 37 °C and 5% CO_2. At least 100 cells per group were imaged on a Leica DMI4000B microscope with a DFC7000T fluorescent camera under a 20× long-working distance air objective. Bright-field and UV channels were used to identify 100 DRG neurons per group by their 10- to 70-μm-diameter circular morphology and large Hoechst-positive nuclei. Three independent experiments were performed.

Real-Time qPCR. qRT-PCR for RAGs was performed as previously described (17). Detailed procedures, including all primers, can be found in *SI Appendix*.

Western Blot. To analyze protein levels in cultured neurons, embryonic DRG neurons were cultured for 6 d. Neurons from three littermate embryos were pooled for each experiment. To assess 17AAG's effect on DLK levels, groups were treated with either 5 μM 17AAG or an equivalent volume of DMSO for either 4 or 8 h. To measure turnover of DLK and SCG10, cycloheximide was added for 4 or 8 h. For all experiments, lysate was collected with sample buffer on ice and analyzed via SDS/PAGE. DLK band intensities of each lane were normalized to the intensity of their corresponding TUJ1 loading controls. Final values are expressed as fold change over time 0. Five independent experiments were performed.

To measure DLK levels of mice in vivo, sciatic nerves were isolated into ice-cold PBS, where the epineurium was quickly removed. Lysate was collected and quantified with a BCA assay kit (Thermofisher). Protein concentrations were equalized among groups and analyzed by Western blot as described above. DLK levels are represented as fold change over DMSO controls.

To assess *Drosophila* protein levels, VNCs were isolated from third-instar larvae and homogenized. VNCs from 10 genetically identical flies were pooled into one lysate to achieve sufficient protein concentration. Lysates were analyzed via SDS/PAGE. Wnd or Hsp83 levels are represented as fold over control animals. This experiment was performed four times. Detailed Western blot procedures, including all antibodies and reagents used, can be found in *SI Appendix*.

Coimmunoprecipitation. HEK-293T cells were cultured to 70–80% confluence and then transfected via polyethylenimine with either empty FUIV [FUGW-ubiquitin promoter-internal ribosome entry site-enhanced YFP (Venus)] vector (72) or FUIV containing flag-tagged DLK. After 2 d, lysate was collected, a portion was saved as input, and the remainder was incubated with anti-flag beads overnight at 4 °C with gentle shaking. After washes and elution, lysates were analyzed by SDS/PAGE. To immunoprecipitate from embryonic DRG neurons, neurons were cultured in six-well plates at a density of three embryos per condition. Lysate was collected, precleared for 30 min with Protein-G Dynabeads (Invitrogen) at 4 °C, and then incubated with mouse anti-DLK antibody (Neuromab clone N377/20; 1:100) or an equivalent amount of mouse IgG antibody (Jackson ImmunoResearch) overnight at 4 °C. Next, each antibody was immunoprecipitated with Protein-G Dynabeads for 1 h at 4 °C. Precipitates were washed, eluted into sample buffer, and analyzed via SDS/PAGE. Detailed procedures, including all antibodies and reagents used, can be found in *SI Appendix*.

***Drosophila* Nerve Crush Assay.** Third-instar larvae were positioned with their ventral surface up, and segmental nerves were pinched through the cuticle for 5 s with Dumostar 5 forceps (12). After 24 h, larvae were filleted open, fixed, immunostained, mounted, and imaged. Images within each experiment were taken with identical gain, which was set using "control injured" flies to avoid oversaturating LacZ signal. The nerves crushed in this assay stem from motor neurons of the dorsal midline, a narrow strip of cells centered in the VNC. The nuclei of these cells were identified via elav. Because *puc-LacZ* contains a nuclear localization sequence, LacZ intensity was quantified in these nuclei for at least seven animals and normalized to uninjured neurons from control flies. A complete list of fly stocks and extended details can be found in *SI Appendix*.

***Drosophila* Synaptic Overgrowth Assay.** Third-instar larvae were filleted open, fixed in Bouin's fixative for 10 min at room temperature, mounted, and imaged. The number of DVGLUT-positive boutons were quantified from 18–23 NMJs at muscle 4 from at least four animals per genotype. Extended details can be found in *SI Appendix*.

Experimental Design and Statistical Analysis. Statistical tests were performed in Prism (GraphPad). All data are presented as mean ± SEM except for Fig. 1*E*, which is shown as mean ± SD to depict the well-to-well variability of the screen. Experiments with two conditions (Figs. 1*E*, 5*F*, and 6 *B* and *C*) were analyzed for statistical significance with a Student's *t* test. One-way ANOVA with a Tukey post hoc test was used to determine significance and correct for multiple comparisons of experiments with three or more groups (Figs. 2 *B* and *D*, 3 *B*–*E*, 6*E*, and 7*B* and *SI Appendix*, Fig. S1). Two-way ANOVA with a Sidak post hoc correction was performed on data in Fig. 5 *B* and *D*, as time and treatment were two independent variables. Asterisks indicate *P* values: $*P < 0.05$, $**P < 0.01$, and $***P < 0.001$; exact values are in the figures. Extended details can be found in *SI Appendix*.

ACKNOWLEDGMENTS. We thank Maxene Ilagan (Washington University High-Throughput Screening Core) for the ICCB Library; Dan Summers for his technical expertise with biochemistry and screen development; and William Buchser, Zach Pincus, and Josiah Gerdts for assisting with development of the screen and CellProfiler pipeline. We also thank the laboratories of J.M. and A.D. for helpful discussions and support. This work was supported by funding from the Philip and Sima Needleman Student Fellowship in Regenerative Medicine (to S.K.-G.) and NIH Grants F31NS101827 (to A.R.), F32NS093962 (to E.F.), NS087562 (to J.M. and A.D.), and NS065053 (to J.M. and A.D.).

1. Bradke F, Fawcett JW, Spira ME (2012) Assembly of a new growth cone after axotomy: The precursor to axon regeneration. *Nat Rev Neurosci* 13:183–193.
2. Farley MM, Watkins TA (2018) Intrinsic neuronal stress response pathways in injury and disease. *Annu Rev Pathol* 13:93–116.
3. Rishal I, Fainzilber M (2014) Axon-soma communication in neuronal injury. *Nat Rev Neurosci* 15:32–42.
4. Abe N, Cavalli V (2008) Nerve injury signaling. *Curr Opin Neurobiol* 18:276–283.
5. Smith DS, Skene JH (1997) A transcription-dependent switch controls competence of adult neurons for distinct modes of axon growth. *J Neurosci* 17:646–658.
6. Klinedinst S, Wang X, Xiong X, Haenfler JM, Collins CA (2013) Independent pathways downstream of the Wnd/DLK MAPKKK regulate synaptic structure, axonal transport, and injury signaling. *J Neurosci* 33:12764–12778.
7. Miller BR, et al. (2009) A dual leucine kinase-dependent axon self-destruction program promotes Wallerian degeneration. *Nat Neurosci* 12:387–389.
8. Shin JE, et al. (2012) Dual leucine zipper kinase is required for retrograde injury signaling and axonal regeneration. *Neuron* 74:1015–1022.
9. Hammarlund M, Nix P, Hauth L, Jorgensen EM, Bastiani M (2009) Axon regeneration requires a conserved MAP kinase pathway. *Science* 323:802–806.
10. Shin JE, Geisler S, DiAntonio A (2014) Dynamic regulation of SCG10 in regenerating axons after injury. *Exp Neurol* 252:1–11.
11. Watkins TA, et al. (2013) DLK initiates a transcriptional program that couples apoptotic and regenerative responses to axonal injury. *Proc Natl Acad Sci USA* 110:4039–4044.
12. Xiong X, et al. (2010) Protein turnover of the Wallenda/DLK kinase regulates a retrograde response to axonal injury. *J Cell Biol* 191:211–223.
13. Michaelevski I, et al. (2010) Signaling to transcription networks in the neuronal retrograde injury response. *Sci Signal* 3:ra53.
14. Shin JE, Cho Y (2017) Epigenetic regulation of axon regeneration after neural injury. *Mol Cells* 40:10–16.
15. Tedeschi A, Bradke F (2013) The DLK signalling pathway–A double-edged sword in neural development and regeneration. *EMBO Rep* 14:605–614.
16. McQuarrie IG, Grafstein B, Gershon MD (1977) Axonal regeneration in the rat sciatic nerve: Effect of a conditioning lesion and of dbcAMP. *Brain Res* 132:443–453.
17. Frey E, et al. (2015) An in vitro assay to study induction of the regenerative state in sensory neurons. *Exp Neurol* 263:350–363.
18. Saijilafu, et al. (2013) PI3K-GSK3 signalling regulates mammalian axon regeneration by inducing the expression of Smad1. *Nat Commun* 4:2690.
19. Zou H, Ho C, Wong K, Tessier-Lavigne M (2009) Axotomy-induced Smad1 activation promotes axonal growth in adult sensory neurons. *J Neurosci* 29:7116–7123.
20. Schopf FH, Biebl MM, Buchner J (2017) The HSP90 chaperone machinery. *Nat Rev Mol Cell Biol* 18:345–360.
21. Taipale M, Jarosz DF, Lindquist S (2010) HSP90 at the hub of protein homeostasis: Emerging mechanistic insights. *Nat Rev Mol Cell Biol* 11:515–528.
22. Neumann S, Woolf CJ (1999) Regeneration of dorsal column fibers into and beyond the lesion site following adult spinal cord injury. *Neuron* 23:83–91.
23. Carpenter AE, et al. (2006) CellProfiler: Image analysis software for identifying and quantifying cell phenotypes. *Genome Biol* 7:R100.
24. Valakh V, Frey E, Babetto E, Walker LJ, DiAntonio A (2015) Cytoskeletal disruption activates the DLK/JNK pathway, which promotes axonal regeneration and mimics a preconditioning injury. *Neurobiol Dis* 77:13–25.
25. Abe N, Borson SH, Gambello MJ, Wang F, Cavalli V (2010) Mammalian target of rapamycin (mTOR) activation increases axonal growth capacity of injured peripheral nerves. *J Biol Chem* 285:28034–28043.
26. Qiu J, Cafferty WB, McMahon SB, Thompson SW (2005) Conditioning injury-induced spinal axon regeneration requires signal transducer and activator of transcription 3 activation. *J Neurosci* 25:1645–1653.
27. Namgung U, et al. (2004) Activation of cyclin-dependent kinase 5 is involved in axonal regeneration. *Mol Cell Neurosci* 25:422–432.
28. Verma P, et al. (2005) Axonal protein synthesis and degradation are necessary for efficient growth cone regeneration. *J Neurosci* 25:331–342.
29. Williams KL, Rahimtula M, Mearow KM (2005) Hsp27 and axonal growth in adult sensory neurons in vitro. *BMC Neurosci* 6:24.
30. Hao Y, et al. (2016) An evolutionarily conserved mechanism for cAMP elicited axonal regeneration involves direct activation of the dual leucine zipper kinase DLK. *eLife* 5:e14048.
31. Qiu J, et al. (2002) Spinal axon regeneration induced by elevation of cyclic AMP. *Neuron* 34:895–903.
32. Patel S, et al. (2015) Discovery of dual leucine zipper kinase (DLK, MAP3K12) inhibitors with activity in neurodegeneration models. *J Med Chem* 58:401–418.
33. Raivich G, et al. (2004) The AP-1 transcription factor c-Jun is required for efficient axonal regeneration. *Neuron* 43:57–67.
34. Bonilla IE, Tanabe K, Strittmatter SM (2002) Small proline-rich repeat protein 1A is expressed by axotomized neurons and promotes axonal outgrowth. *J Neurosci* 22:1303–1315.
35. Whitesell L, Lindquist SL (2005) HSP90 and the chaperoning of cancer. *Nat Rev Cancer* 5:761–772.
36. Taipale M, et al. (2012) Quantitative analysis of HSP90-client interactions reveals principles of substrate recognition. *Cell* 150:987–1001.
37. Walker LJ, et al. (2017) MAPK signaling promotes axonal degeneration by speeding the turnover of the axonal maintenance factor NMNAT2. *eLife* 6:e22540.
38. Citri A, et al. (2006) Hsp90 recognizes a common surface on client kinases. *J Biol Chem* 281:14361–14369.
39. Shin JE, et al. (2012) SCG10 is a JNK target in the axonal degeneration pathway. *Proc Natl Acad Sci USA* 109:E3696–E3705.
40. Biamonte MA, et al. (2010) Heat shock protein 90: Inhibitors in clinical trials. *J Med Chem* 53:3–17.
41. Valakh V, Walker LJ, Skeath JB, DiAntonio A (2013) Loss of the spectraplakin short stop activates the DLK injury response pathway in Drosophila. *J Neurosci* 33:17863–17873.
42. Martín-Blanco E, et al. (1998) Puckered encodes a phosphatase that mediates a feedback loop regulating JNK activity during dorsal closure in Drosophila. *Genes Dev* 12:557–570.
43. Collins CA, Wairkar YP, Johnson SL, DiAntonio A (2006) Highwire restrains synaptic growth by attenuating a MAP kinase signal. *Neuron* 51:57–69.
44. Wan HI, et al. (2000) Highwire regulates synaptic growth in Drosophila. *Neuron* 26:313–329.
45. Ghosh AS, et al. (2011) DLK induces developmental neuronal degeneration via selective regulation of proapoptotic JNK activity. *J Cell Biol* 194:751–764.
46. Chandran V, et al. (2016) A systems-level analysis of the peripheral nerve intrinsic axonal growth program. *Neuron* 89:956–970.
47. Chen L, et al. (2011) Axon regeneration pathways identified by systematic genetic screening in C. elegans. *Neuron* 71:1043–1057.
48. Loh SH, Francescut L, Lingor P, Bähr M, Nicotera P (2008) Identification of new kinase clusters required for neurite outgrowth and retraction by a loss-of-function RNA interference screen. *Cell Death Differ* 15:283–298.
49. Nix P, et al. (2014) Axon regeneration genes identified by RNAi screening in C. elegans. *J Neurosci* 34:629–645.
50. Smith RP, et al. (2011) Transcriptional profiling of intrinsic PNS factors in the postnatal mouse. *Mol Cell Neurosci* 46:32–44.
51. Usher LC, et al. (2010) A chemical screen identifies novel compounds that overcome glial-mediated inhibition of neuronal regeneration. *J Neurosci* 30:4693–4706.
52. Li H, et al. (2016) Protein prenylation constitutes an endogenous brake on axonal growth. *Cell Rep* 16:545–558.
53. Perlson E, et al. (2005) Vimentin-dependent spatial translocation of an activated MAP kinase in injured nerve. *Neuron* 45:715–726.
54. Nix P, Hisamoto N, Matsumoto K, Bastiani M (2011) Axon regeneration requires coordinate activation of p38 and JNK MAPK pathways. *Proc Natl Acad Sci USA* 108:10738–10743.
55. Frey E, Karney-Grobe S, Krolak T, Milbrandt J, DiAntonio A (2018) TRPV1 agonist, capsaicin, induces axon outgrowth after injury via Ca^{2+}/PKA signaling. *eNeuro* 5: ENEURO.0095-18.2018.
56. Bremer J, Skinner J, Granato M (2017) A small molecule screen identifies in vivo modulators of peripheral nerve regeneration in zebrafish. *PLoS One* 12:e0178854.
57. Saibil H (2013) Chaperone machines for protein folding, unfolding and disaggregation. *Nat Rev Mol Cell Biol* 14:630–642.
58. Benitez MJ, Sanchez-Ponce D, Garrido JJ, Wandosell F (2014) Hsp90 activity is necessary to acquire a proper neuronal polarization. *Biochim Biophys Acta* 1843:245–252.
59. Gerges NZ, et al. (2004) Independent functions of hsp90 in neurotransmitter release and in the continuous synaptic cycling of AMPA receptors. *J Neurosci* 24:4758–4766.
60. Luo W, Sun W, Taldone T, Rodina A, Chiosis G (2010) Heat shock protein 90 in neurodegenerative diseases. *Mol Neurodegener* 5:24.
61. Wang Z, et al. (2013) The EBAX-type Cullin-RING E3 ligase and Hsp90 guard the protein quality of the SAX-3/Robo receptor in developing neurons. *Neuron* 79:903–916.
62. Ma CH, et al. (2011) Accelerating axonal growth promotes motor recovery after peripheral nerve injury in mice. *J Clin Invest* 121:4332–4347.
63. Willis D, et al. (2005) Differential transport and local translation of cytoskeletal, injury-response, and neurodegeneration protein mRNAs in axons. *J Neurosci* 25: 778–791, and erratum (2010) 30:np.
64. Le Pichon CE, et al. (2017) Loss of dual leucine zipper kinase signaling is protective in animal models of neurodegenerative disease. *Sci Transl Med* 9:eaag0394.
65. Pozniak CD, et al. (2013) Dual leucine zipper kinase is required for excitotoxicity-induced neuronal degeneration. *J Exp Med* 210:2553–2567.
66. Yan D, Jin Y (2012) Regulation of DLK-1 kinase activity by calcium-mediated dissociation from an inhibitory isoform. *Neuron* 76:534–548.
67. Babetto E, Beirowski B, Russler EV, Milbrandt J, DiAntonio A (2013) The Phr1 ubiquitin ligase promotes injury-induced axon self-destruction. *Cell Rep* 3:1422–1429.
68. Brace EJ, Wu C, Valakh V, DiAntonio A (2014) SkpA restrains synaptic terminal growth during development and promotes axonal degeneration following injury. *J Neurosci* 34:8398–8410.
69. Nakata K, et al. (2005) Regulation of a DLK-1 and p38 MAP kinase pathway by the ubiquitin ligase RPM-1 is required for presynaptic development. *Cell* 120:407–420.
70. Huntwork-Rodriguez S, et al. (2013) JNK-mediated phosphorylation of DLK suppresses its ubiquitination to promote neuronal apoptosis. *J Cell Biol* 202:747–763.
71. Meijering E, et al. (2004) Design and validation of a tool for neurite tracing and analysis in fluorescence microscopy images. *Cytometry A* 58:167–176.
72. Araki T, Sasaki Y, Milbrandt J (2004) Increased nuclear NAD biosynthesis and SIRT1 activation prevent axonal degeneration. *Science* 305:1010–1013.